EurJOC

European Journal of Organic Chemistry

Accepted Article

Title: Synthetic β-cyclodextrin dimers for squaraine binding: Effect of host architecture on photophysical properties, aggregate formation and chemical reactivity

Authors: Sauradip Chaudhuri, Molly Verderame, Teresa L. Mako, Y. M. Nuwan D. Y. Bandara, Ashvin I. Fernando, and Mindy Levine

WILEY-VCH

FULL PAPER

Synthetic β-cyclodextrin dimers for squaraine binding: Effect of host architecture on photophysical properties, aggregate formation and chemical reactivity

Sauradip Chaudhuri, Molly Verderame, Teresa L. Mako, Y. M. Nuwan D. Y. Bandara, Ashvin I. Fernando and Mindy Levine*[a]

Dedicated in memory of the father of biomimetic chemistry, a giant in the field of cyclodextrin chemistry, and the former Ph.D. advisor of M.L., Professor Ronald Breslow.

Abstract: Reported herein is the synthesis and application of three novel β-cyclodextrin dimer hosts for the complexation of near infrared (NIR) squaraine dyes in aqueous solution. A series of eight different N-substituted N-methyl anilino squaraine dyes with variable terminal groups are investigated, with an optimal n-hexyl substituted squaraine guest demonstrating binding constants orders of magnitude higher than the other squaraine-host combinations and comparable to literature-reported systems. Moreover, hydrophobic complexation of the squaraine dyes with the β-cyclodextrin dimer hosts causes drastic changes in the squaraine's photophysical properties, propensity for aggregation and susceptibility to hydrolytic decay.

Introduction

The complexation of small molecule guests inside a variety of supramolecular hosts has been extensively reported in the literature. Examples of such hosts include cyclodextrins,[1] which bind guests primarily via hydrophobic encapsulation inside the hydrophobic cavity;[2] cucurbiturils (CBs),[3] which bind guests via electrostatic interactions with the highly polarized carbonyl groups that line the CB rims as well as via hydrophobic association;[4] and synthetic macrocycles[5] and cavitands,[6] whose structures vary widely as a result of synthetic manipulations.

Previous work by our group has focused on the use of cyclodextrin complexation to develop highly sensitive and selective fluorescence-based detection methods for multiple classes of toxicants, including polycyclic aromatic hydrocarbons (PAHs),[7] polychlorinated biphenyls (PCBs),[8] aromatic pesticides,[9] aliphatic alcohols,[10] and aromatic oil-spill components.[11] These detection methods operate via cyclodextrin-promoted fluorescence energy transfer,[12] in cases where the toxicant is photophysically active and a competent energy donor, or via cyclodextrin-promoted fluorescence modulation,[13] in cases where the toxicant is not photophysically active but still binds in cyclodextrin and promotes proximity-induced, analyte-specific changes in the fluorophore emission. No previous work in our group has reported the use of higher order cyclodextrin architectures for detection applications, despite the fact that such architectures have the potential to exhibit significantly enhanced binding affinities.[14]

One group of guests that is known to bind well in cyclodextrins is squaraine fluorophores,[15] which contain a common cyclobutene-dione core.[16] The unique electronic structure of the squaraine fluorophore leads to high extinction coefficients,[17] narrow Stokes shifts, and high quantum yields,[18] with absorption and emission maxima often in the near-infrared spectral region. Squaraine fluorophores have significant potential in detection applications, as a result of the limited interference of other analytes in the near-infrared spectral region.[19] Moreover, squaraine binding in cyclodextrin hosts often results in changes in the absorption and emission spectra of the squaraine that can be used for sensing applications.[20]

Reported herein is the rational design and synthesis of dimeric cyclodextrin architectures, their ability to bind squaraine fluorophores with extremely high binding constants, and the effects of such binding on the squaraines' photophysical properties, propensity for aggregate formation, and reactivity towards hydrolysis. Detailed structure-property relationships are invoked to understand the effects of the structural architectures of the dimers on squaraine guests with variable-length terminal alkyl chains.
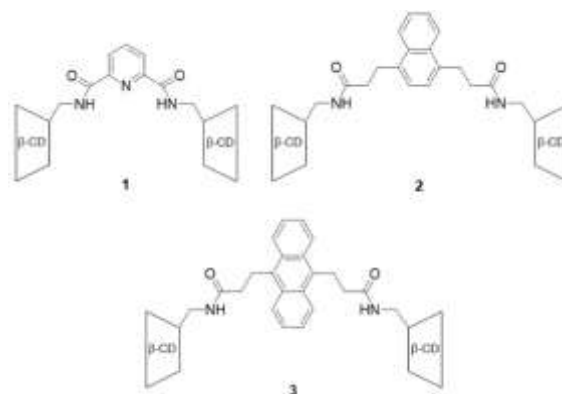
[a]   S. Chaudhuri, M. Verderame, T. L. Mako, Y. M. N. D. Y. Bandara, A. I. Fernando, M. Levine
Department of Chemistry
University of Rhode Island
140 Flagg Road, Kingston, RI 02881
E-mail: mindy.levine@gmail.com; mlevine@chm.uri.edu
URL: https://www.chm.uri.edu/levinegroup/webpages/index.html
Supporting information for this article is given via a link at the end of the document.

Figure 1. Structures of new cyclodextrin dimers **1-3**.

FULL PAPER

Results and Discussion

Host design and properties

Three novel, covalently linked β-cyclodextrin dimers (compounds **1-3**) with aromatic linkers were synthesized via the coupling of activated amide derivatives with two equivalents of monofunctionalized β-cyclodextrin. While compound **1** incorporates a rigid 2,6-pyridine diamide linker, compounds **2** and **3** incorporate flexible 1,4-naphthalene and 9,10-anthracene dipropylamide linkers, respectively (Figure 1). The three linker architectures were chosen to determine the effect of a heteroaromatic moiety (compound **1**), increasing sizes of the aromatic core (compound **2** vs. compound **3**), and differences in the linker flexibility (compound **1** vs. compounds **2** and **3**) on the binding properties of β-cyclodextrin dimers. Such flexibility can be seen in the energy-minimized structures of compounds **1-3**, obtained via PM3-level computations: whereas compound **1** exhibits an open structure as a result of its limited flexibility, compounds **2** and **3** are sufficiently flexible to fold in, exhibiting a closed, sandwich-like structure (Figure 2).
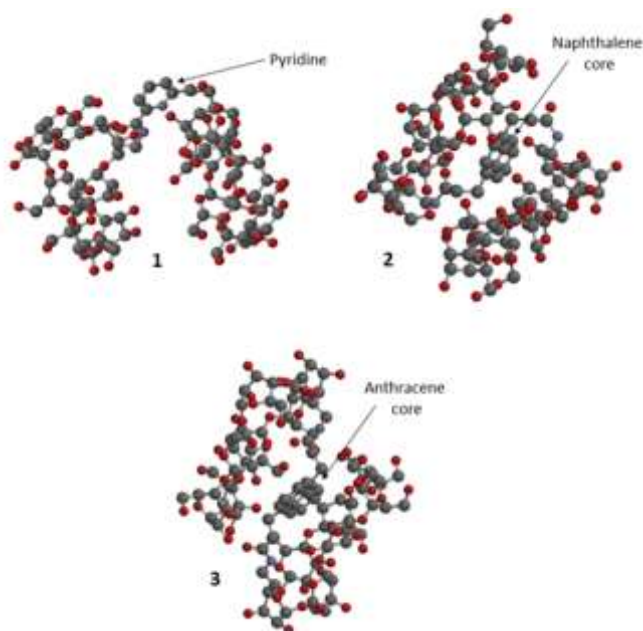

Figure 2. Energy minimized semi-empirical PM3-levl calculations of hosts **1-3**.

Moreover, dimers **1-3** are photophysically active, as a result of the incorporation of fluorescent linkers. While the integrated fluorescence intensities of compounds **2** and **3** increased linearly with increased dimer concentration, the fluorescence intensity of compound **1** displayed non-linear behaviour (see ESI for more details). This is due to the rigid conformation of **1,** which facilitates intermolecular aggregation, especially at elevated concentrations in aqueous solutions; such aggregation, in turn, results in the development of different fluorescence profiles with complicated spectroscopic trends.
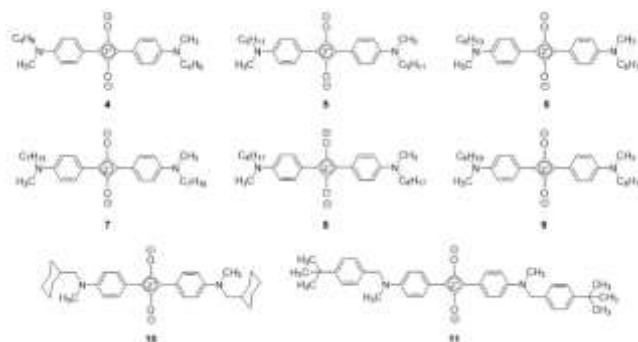

Figure 3. Structures of *N*-substituted *N*-methylanilino squaraine dyes **4-11** (note that the alkyl substituents in compounds **4-9** are all straight chain *n*-alkanes).

Eight squaraine guests (compounds **4-11**, Figure 3) were synthesized via the condensation of squaric acid and *N*-substituted *N*-methylanilines following a general procedure previously reported for the synthesis of similar species.[21] Six of the squaraines reported herein incorporate straight chain alkyl groups from *n*-butyl to *n*-nonyl (compounds **4-9**), with a cyclic substituent (compound **10**) and a *tert*-butyl substituted benzene (compound **11**) included in the other two structures (Figure 3). All of the cyclodextrins and squaraines were fully characterized via spectroscopic methods.
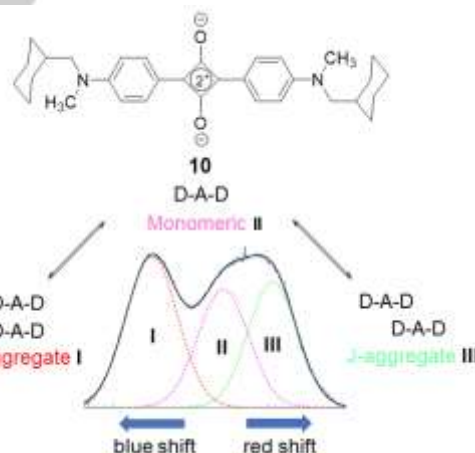

Figure 4. Illustration of Donor-Acceptor-Donor (D-A-D) structure of squaraine dye **10**, resulting in the formation of intense H-aggregate (blue-shifted) and J-aggregate (red-shifted) bands, especially in aqueous solution

Complexation-driven spectroscopic changes

Squaraines can exist in their monomeric form under certain conditions, but are particularly prone to aggregation (as either H-aggregates or J-aggregates) due to their highly planar structures (Figure 4).[22] Cyclodextrin complexation of the squaraines is reported to affect the equilibrium between the monomeric and aggregated states, with squaraines in β-cyclodextrin complexes stabilized in their monomeric states, and squaraines in γ-cyclodextrin complexes stabilized as dimers.[23] In our system, the

monomeric squaraine species (shown in Figure 5 for compound **6**) shows a UV-visible absorption peak with a maximum around 650 nm (band II), with the H-aggregate absorbing between 500 and 600 nm (band I), and the J-aggregate showing a strong absorption in the near-infrared spectral range (band III). These separate absorption profiles enable quantification of the prevalence of both H- and J-aggregates for varying squaraine concentrations in presence of dimers **1-3** (Figure 5).
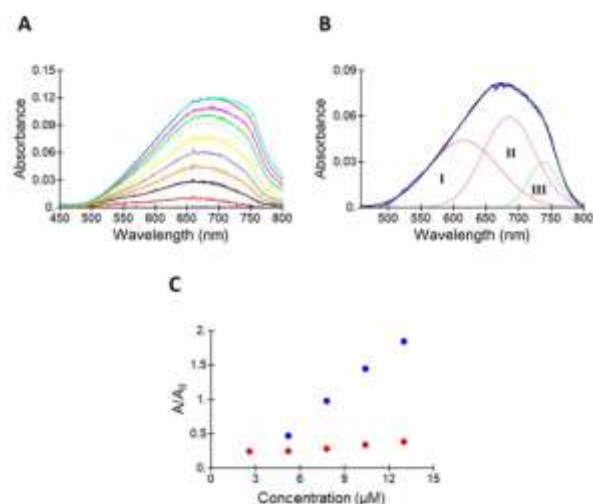

Figure 5. Spectral deconvolution for investigation of H- and J-aggregate formation with increasing concentrations of squaraine **6**. (A) UV-vis spectra of increasing concentrations of squaraine **6** ([**6**] = 1.3 μM (red), 2.6 μM (black), 3.9 μM (orange), 5.2 μM (grey), 6.5 μM (yellow), 7.8 μM (light grey), 9.1 μM (green), 10.4 μM (pink), 11.7 μM (brown), 13.0 μM (blue); (B) Representative deconvoluted spectra of squaraine **6** ([**6**] = 7.8 μM, H-aggregate (I), Monomeric state (II), J-aggregate (III)); (C) Plot of H- aggregate prevalence (ratio I/II, blue) and J- aggregate prevalence (ratio III/II, red) against dye concentration for squaraine **6**.

Of note, among squaraines **4-9**, the shorter alkyl chain-substituted squaraines **4-6** showed predominantly H-aggregate formation, whereas the longer alkyl chain-substituted squaraines **7-9** showed mostly J-aggregation. Of the two *N*-substituted squaraines with cyclic substituents (compounds **10** and **11**), H-aggregation was slightly more dominant than J-aggregation for compound **10**, whereas compound **11** favoured J-aggregation. Moreover, the cyclodextrin dimers had a substantial effect in disrupting H-aggregation in the smaller squaraines, whereas lower effects were observed in the cyclodextrin-induced disruption of aggregation of the larger squaraines.

While compounds **1** and **2** caused a significant decrease in the H-band of squaraine **6** (Figure 6A-C), virtually no aggregation was observed in the presence of compound **3** (Figure 6D). The effect of host dimer **3** was also very pronounced for guest squaraine **10**, and resulted in a marked decrease in both the H-aggregate and J-aggregate absorption bands (Figure 7). Squaraines with *N*-terminal substituents shorter than *n*-hexyl (i.e. **4** and **5**) showed a sharp rise in the H-band with flexible dimer hosts **2** (for squaraine **4**) and **3** (for squaraines **4** and **5**) at low squaraine concentrations,

which gradually diminished with increasing concentrations of the dye. This spectroscopic behaviour can be explained by the ability of dimers **2** and **3** to bind two squaraines, forming a stable 1:2 host-guest complex.
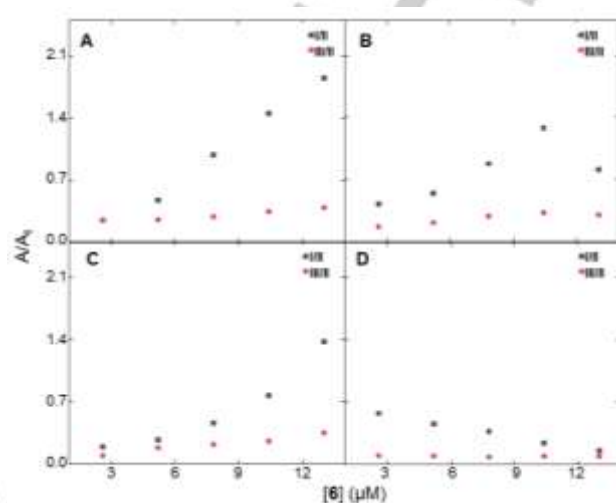

Figure 6. Plots of the ratios of H-aggregate (**I/II**, grey) and J-aggregate (**III/II**, orange) to monomeric squaraine vs concentrations of squaraine **6** for (A) control (no host); (B) compound **1** (8 μM); (C) compound **2** (8 μM); and (D) compound **3** (8 μM).
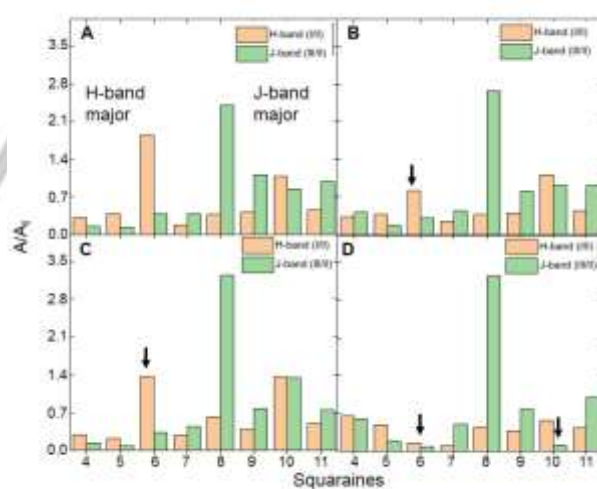
Figure 7. Bar graphs showing H and J-aggregate formations for various squaraines in presence of: (A) no cyclodextrin (control); (B) **1** (8 μM); (C) **2** (8 μM); and (D) **3** (8 μM). Downward arrows indicate the significant reduction of aggregate formation for the squaraines **6** and **10**.

Complexation-induced effects on squaraine hydrolysis

The hydrolyses of squaraines **4-11** in aqueous solution at room temperature were studied in the presence of equimolar amounts of dimers **1-3**. These reactions follow first-order reaction kinetics, as shown in Equation 1, below:

FULL PAPER

$$A/A_0 = e^{-kt} + C \qquad \text{(Equation 1)},$$

where A is the integrated area of absorption at a given time, A_0 is the initial integrated area of absorption, k is the exponential decay constant, and C is the equilibrium concentration of the decaying squaraine species (Figure 8A).

The linear form of Equation 1 can also be expressed in logarithmic form, as shown in Equation 2, below:

$$-\text{Log}_{10}(A/A_o - C) = kt - \text{Log}_{10}(1-C) \qquad \text{(Equation 2)},$$

where the intercept and the slope is given by $-\text{Log}_{10}(1-C)$ and decay constant k respectively (Figure 8B).

Figure 8. (A) Plot of A/A_o vs time for first-order exponential hydrolytic decay of squaraine **6** measured at every half an hour over 5 hours. **(B)** Linear plot for first order exponential hydrolytic decay of squaraine **6** for (i) control; (ii) compound **1**; (iii) compound **2**; and (iv) compound **3** (slope of the plot is a measure of the exponential decay constant k; intercept c of the plot is a measure of the aggregate concentration C)
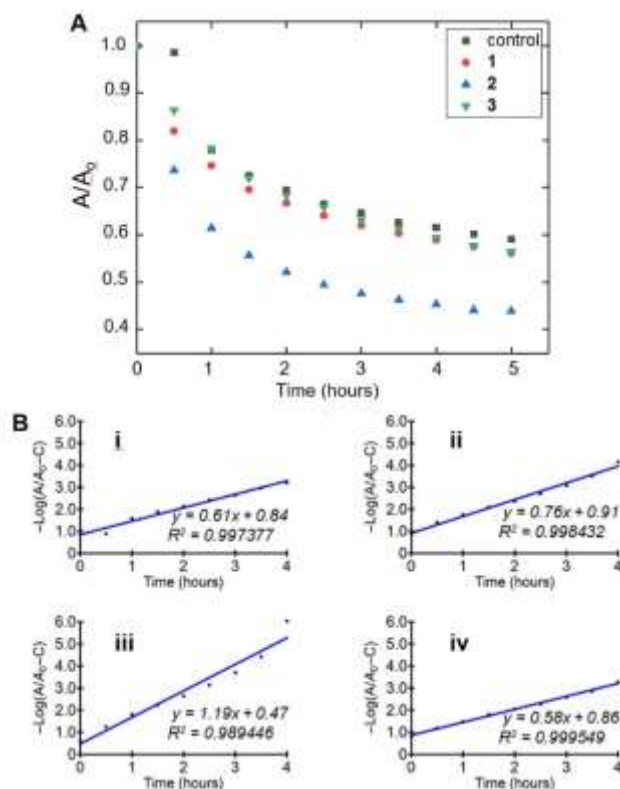
In Equation 1, the two constants C and k are independent parameters that indicate the extent of hydrolysis, by providing the equilibrium squaraine concentration, and the rate of hydrolysis, by providing the first-order rate constant. They can be related to each other via the theoretical hydrolytic protection parameter, T, defined in Equation 3, below:

$$T = -\text{Log}(1-C)/k \qquad \text{(Equation 3)}$$

where -Log(1-C) is the Y-intercept and k is the slope of the line. Higher T values mean greater degrees of hydrolytic protection, whereas lower T values indicate increased rates of decay.

We plotted the ratio of T in the presence of cyclodextrin hosts **1-3** (T_{dimer}) to T in the absence of any host ($T_{control}$) (Figure 9), noting

that a ratio value of 1 would represent no effect of the host on the rate or extent of hydrolysis. Notably, squaraines in the presence of host **1** demonstrated the lowest effects of complexation on hydrolysis behaviours (as indicated by ratios closest to **1**). For most squaraines, the presence of host **2** led to moderate protection from hydrolysis, indicated by ratio values slightly higher than **1**, and host **3** conferred substantial hydrolytic protection to the squaraines.
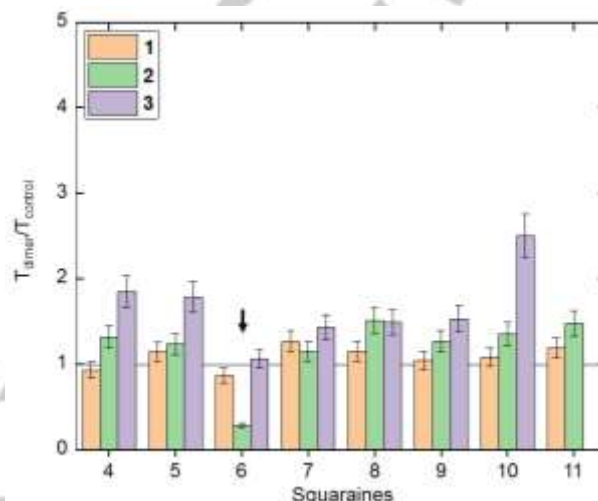
Figure 9. Bar graph plot of the ratio of hydrolytic protection ($T_{dimer}/T_{control}$) of squaraines in presence of the dimers (**1-3**). (T is defined in Equation 3; downward arrows indicate the larger extent of hydrolytic decay for the squaraines **6**; errors are calculated from standard deviations of c and k from the linear plots and error bars are within 10% of the calculated T values).

Figure 10. (A) Generalized representation of the structure of squaraines dyes (**4-11**) depicting the relatively hydrophilic (red) and hydrophobic (blue) parts of the molecule. **(B)** Schematic representation of the host-guest association in dimer **1**, showing the H-bonding interaction of the two amide linkers to the oxoanion of the squaraine core.

FULL PAPER

Notably, squaraine **6** in the presence of host **2** demonstrated an exception to this general trend, and displayed markedly increase hydrolysis rates in the pre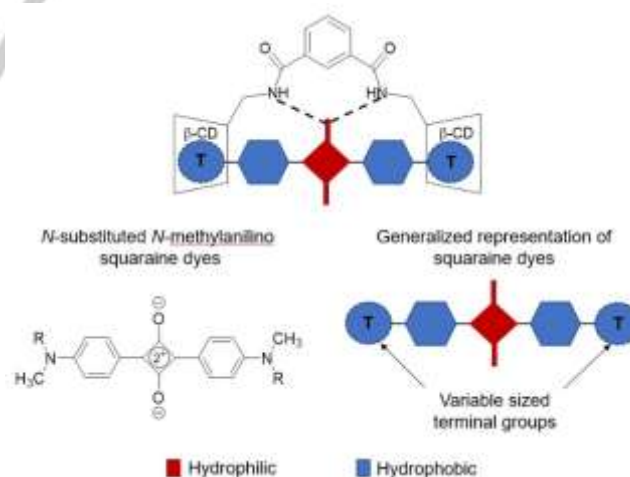sence of the host compared to in its absence. This aberrant behaviour is a result of the optimal fit between the squaraine **6** guest and the β-cyclodextrin host cavities, which enables each β-cyclodextrin unit to activate the electrophilic squaraine for hydrolysis via hydrogen-bonding interactions with the oxoanions upon complexation (Figure 10). Host **2** was particularly effective at increasing the rates of hydrolysis, as a result of the greater conformational flexibility of the linker in compound **2**, which enables the β-cyclodextrin units to access the squaraine core and promote hydrolysis. Although dimer **3** has a relatively similar architecture, the tethering of the methylene linkers to the 9,10-positions of the anthracene moiety constrains the conformational flexibility.

A particularly high degree of hydrolytic protection was observed for squaraines **10** and **11** with host **3**, which is a result of the conformational changes induced by the binding of the bulky cycloalkyl and aromatic substituents in the cyclodextrin cavities. These changes further stabilize the dimer-squaraine complex, resulting in highly effective protection. Both complexes (**3 + 10** and **3 + 11**) were studied computationally and shown to have different conformations than the *n*-alkyl substituted guest **6** (Figure 11).
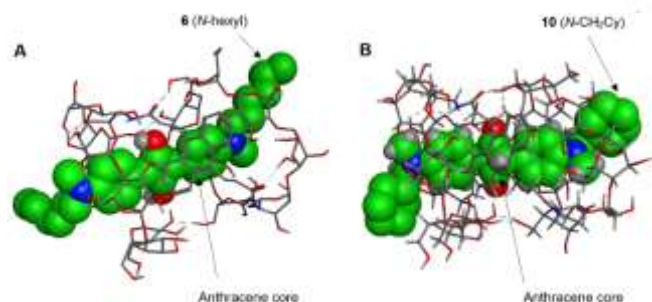

Figure 11. Energy minimized (semi-empirical PM3) computational models for (A) squaraine-dimer combination (**3 + 6**); and (B) squaraine-dimer combination (**3 + 10**), illustrating the different location of the anthracene core with respect to the electrophilic squaraine core in both the cases.

Another combination of note was squaraine **11** with dimer **3**, in which the hydrolytic decay of the squaraine exhibited zero-order behaviour. This is likely due to the fact that the complexation-induced conformational changes minimize complex dissociation, which in turn limits the availability of free squaraine **11**. As a result, the rate of hydrolysis becomes independent of the overall squaraine concentration. In fact, all hosts **1-3** when complexed with squaraine **11** led to near zero-order behaviour as well, pointing to the likelihood of the interactions between β-cyclodextrin and the *tert*-butylphenyl substituent as key for inducing this kinetic behaviour.

For all squaraines except for **6** and **7**, which are particularly easily hydrolysed in the presence of dimer **2** due to optimal steric matching, the general trend in the complexation-induced hydrolytic protection follows the order **3 > 2 > 1**. This trend can be explained based on the conformation of the host-guest (dimer-

squaraine) complex. While squaraines **4** and **5** form stable 1:2 host-guest complex with **3**, squaraines **6-9** thread into the β-cyclodextrin cavities and adapt a pseudo-rotaxane geometry. Moreover, as a result of the closed structures of β-cyclodextrin dimer hosts **2** and **3**, they are more able than host **1** to protect the electrophilic squaraine core against hydrolysis.

Fluorescence titration of cyclodextrin dimer hosts

The guest-induced fluorescence changes of the dimers **1-3** ([dimer] = 5 x 10^{-7} M) was studied in presence of increasing concentrations of squaraines **4-11**.[24] Importantly, the observed behaviours are intimately dependent on the specific interactions between each squaraine guest and cyclodextrin host, which makes general trends challenging to elucidate.

While the fluorescence intensity of dimer **1** decreased with increasing concentrations of squaraine guests (for all guests except compounds **4** and **10**), the intensities of dimers **2** and **3** increased with increasing amounts of squaraine (except for guests **9-11** with dimer **3**). The smallest squaraine **4** formed stable 1:2 host-guest association complex with all three hosts, while **5** exhibited a 1:2 binding with only **3**. In contrast, the bulkier squaraines (**6-11**) formed 1:1 host-guest binding model with all the three dimers (**1-3**) in all cases (Table 1).

Table 1. Calculated association constant values for β-cyclodextrin dimer hosts (**1-3**) with squaraine guests (**4-11**)

Guest	Host 1	Host 2	Host 3
4	[b]7.5 (1.3) x 10^{14}	[b]8.8 (2.4) x 10^{13}	[b]2.3 (0.4) x 10^{13}
5	[a]2.7 (0.5) x 10^{6}	[a]2.6 (0.4) x 10^{6}	[b]4.5 (1.0) x 10^{13}
6	[a]3.5 (0.5) x 10^{6}	[a]3.5 (1.2) x 10^{5}	[a]2.3 (0.1) x 10^{8}
7	[a]1.5 (0.7) x 10^{6}	[a]2.1 (0.8) x 10^{5}	[a]4.1 (0.5) x 10^{6}
8	[a]4.5 (0.8) x 10^{6}	[a]3.1 (0.1) x 10^{5}	[a]3.2 (0.4) x 10^{7}
9	[a]6.6 (0.8) x 10^{6}	[a]2.4 (0.7) x 10^{5}	[a]8.1 (0.5) x 10^{5}
10	[a]1.7 (0.4) x 10^{5}	[a]4.2 (1.0) x 10^{5}	[a]2.4 (0.6) x 10^{6}
11	[a]1.2 (0.2) x 10^{7}	[a]1.0 (0.1) x 10^{6}	[a]3.0 (0.2) x 10^{6}

[a] Association constant (M^{-1}) values are reported for 1:1 host-guest complex formation in aqueous phosphate buffered saline (PBS) solution. [b] Association constant (M^{-2}) values are reported for 1:2 host-guest complex formation in aqueous PBS solution. All values are calculated as an average of at least three trials. Error values are included in parentheses.

The association constant values for 1:2 host-guest complexes of squaraine **4** (shown in the top row of Table 1) followed the trend **1>2>3**, with the association constants of first guest binding events, K_1 (2.8(0.3) x 10^{3} M^{-1}, 1.6(0.4) x 10^{4} M^{-1}, and 3.3(0.4) x 10^{3} M^{-1}, respectively), being several orders of magnitude lower than that of the association constants of the second guest binding events, K_2 (2.7(0.4) x 10^{11} M^{-1}, 5.4(0.8) x 10^{9} M^{-1}, and 7.1(0.9) x 10^{9} M^{-1}, respectively). This means that the binding of the first squaraine **4** guest renders the host cavity much more receptive to the second guest. While the association constant values for most of the

FULL PAPER

cyclodextrin-squaraine combinations were on the order of 10^5-10^7 M^{-1}, squaraine **6** exhibited extraordinary affinity for dimer host **3**, with calculated association constants of 10^8 M^{-1}. The association constant values are comparable in magnitude to previously reported values for host-guest binding with cyclodextrin dimers.25 Among the straight chain alkyl-substituted squaraines, compounds **5** and **6** have optimal sizes and hydrophobicities to bind in hosts **2** and **3**, respectively. Squaraines with longer alkyl chain substituents (**7-9**) exhibited association constants that were one and two orders of magnitude lower with dimers **2** and **3**, respectively. This trend is likely due to less optimal steric matching with the host cavity for the larger squaraines.

A comparison of squaraine guests **10** and **11** revealed that compound **11** exhibited higher association constants because of the *tert*-butylphenyl substituent, which has been reported to bind strongly in β-cyclodextrin (K_a = 1.6 x 10^4 M^{-1}).25 Despite structural similarities between hosts **2** and **3**, the association constants for compound **2** are low for most of the squaraines compared to those observed for compound **3** (Figure 12). This differential behaviour may be a result of the greater hydrophobicity of the anthracene unit in compound **3**, which in turn contributes to increased cooperativity of the β-cyclodextrin units in forming a stable 1:1 host-guest complex.
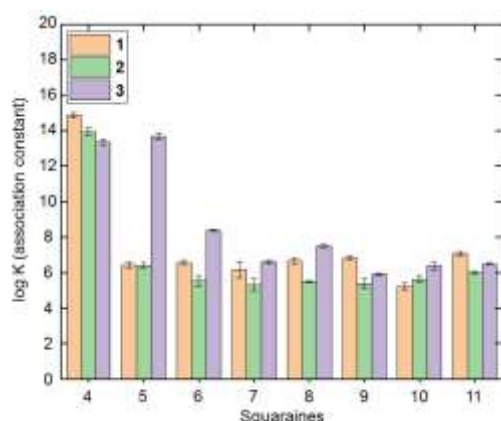

Figure 12. Plot of log K (association constants) versus *N*-substituted anilino squaraines (**4-11**) for β-cyclodextrin dimer hosts (**1-3**). Values for squaraine **4** (for all hosts) and squaraine **5** (for host **3**) are for 1:2 host-guest complexes. (Error bars that are shown represent the error of least three trials).

The changes in the fluorescence of the dimer **3** upon addition of squaraines **6** and **10** were further analysed to understand the different complexation modes of the squaraine guests. While compound **6** is an example of the *n*-alkyl squaraines that caused an increase in the fluorescence of dimer **3**, compound **10** is an example of the bulky *N*-substituted squaraines that caused a decrease in the fluorescence emission of compound **3** with complex formation. These opposing trends were explained by computational energy minimized models of host-guest complexes of host **3** with guest **6** compared to host **3** with guest **10**. Unlike flexible n-alkyl substituents in compound **6**, the bulky substituent in compound **10** causes a significant conformational change of

host **3**, resulting in the anthracene-containing linker interacting closely with the electron deficient core of guest **10** and facilitating excited state energy transfer. This host-guest conformation was also noted for **11** with bulky *tert*-butylphenyl substituents. In contrast, complexation of guest **6** leads to a relatively open structure, where the anthracene core is displaced from the host cavity (Figure 11, *vide supra*).

Computational Modelling

The stabilities of the 1:1 cyclodextrin: squaraine complexes were calculated using PM3 calculations (with a semi-empirical force field) for host **3** with guests **6**, **10** and **11**. Guest **6** complexation with all hosts **1-3** was also investigated to determine the oxoanion-amide distances in host-guest complexes (Table 2). The calculated negative stabilization energies indicate that the squaraine guests thread inside the host cavity (**1-3**) to form a stable host-guest association complex. Interestingly, complexes of host **3** with guests **10** and **11** were substantially more stable than the complex formed between host **3** and *n*-hexyl-substituted squaraine **6**.

Table 2. Calculated stabilization energy values for β-cyclodextrin dimer hosts (**1-3**) with squaraine guests **10**,**11** (with host **3**) and **6** (with hosts **1**,**2**, and **3**) assuming 1:1 complexation.

E_{host}[a] (KJ/mol)	E_{guest}[b] (KJ/mol)	$E_{complex}$[c] (KJ/mol)	$\Delta E_{complex}$[d] (KJ/mol)	d_2-d_1[e] (Å)
	11 = 215.4	-11497.7	-53.0	4.37
3 = -11660.1	**10** = -3.4	-11689.2	-25.7	4.31
	6 = -42.1	-11719.5	-17.3	4.35
2 = -11735.8	**6** = -42.1	-11841.3	-63.4	0.86
1 = -11814.9	**6** = -42.1	-11890.9	-33.9	2.31

[a] Energy of formation of the host. [b] Energy of formation of the guest. [c] Energy of formation of the 1:1 host-guest complex. [d] Stabilization energy of the 1:1 host-guest complex. [e] Difference in the 1st and 2nd oxoanion-amide pair bond lengths (Figure 13). Energy minimized models were carried out using PM3 level calculations with semi-empirical force field. Values of d_1 (distance of the 1st oxoanion-amide pair bond) and d_2 (distance of the 2nd oxoanion-amide pair bond) are included in Table S19 in the ESI.

The distances of the two oxoanion-amide pairs (d_1 and d_2, Figure 13) were compared to determine the precise position of the electrophilic squaraine core, and in particular to distinguish between two possible modes of interaction: (a) interaction in which the two amide groups of the linker interact closely with one oxoanion of the squaraine core, resulting in a significant difference between the two measured distances (option I, Figure 13); or (b) interaction in which the two amide groups of the linkers interact equally with both oxoanions of the squaraine core, resulting in approximately equivalent distances (option II, Figure 13). Notably, the dual hydrogen bonding interactions available in option II are expected to provide substantially more electrophilic activation than option I. The observed trend in the difference of the measured distances (d_2 - d_1) for squaraine **6** for all the complexes was **3**>**1**>**2**, and supports option (b) as the more likely

FULL PAPER

mode of interaction (**2**-SQ, *II*, Figure 13) This observation explains the anomalously high rate of hydrolysis of squaraine **6** in presence of host **2**, owing to the enhanced electron deficient nature of the squaraine core making it susceptible to hydrolytic attack.
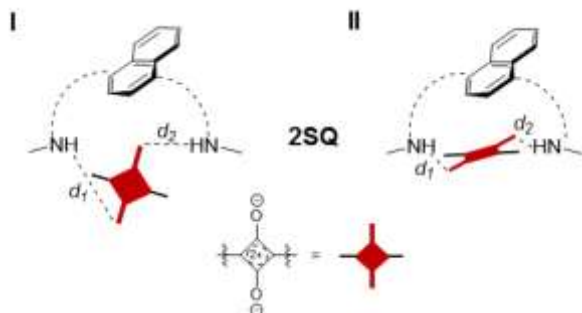

Figure 13. Possible modes of squaraine core-linker interactions resulting in a significantly large (case *I*) and minimum (case *II*) difference in the measured oxoanion-amide distances (d_2 - d_1).

Synthetic tetralactam macrocycle-based squaraine rotaxanes have been reported in the literature with association constants 1000 times greater in aqueous solution compared to organic solvents. [26] Unlike tetralactam macrocycles, where the rational design of the macrocycles is primarily targeted at hydrogen bonding-induced stabilization of the squaraine core, the complexation of squaraines in β-cyclodextrin dimers is entirely driven by hydrophobicity of the squaraine guests (**4-11**) in the aqueous medium, but results in substantial hydrogen bonding interactions. The hydrophobic nature of the complexation of **3** and **6** was further evident from the two separate spots visible on the TLC plate after eluting an aqueous solution of **3** and **6** with a mixture (1:9) of methanol in chloroform (see ESI). These results mean that the squaraine guest is not bound in the host in the absence of water, because of the inability to use hydrophobic binding under such conditions. Previous work on squaraine encapsulation,[26] in contrast, which relies on hydrogen bonding of the oxoanions by the macrocycles, results in one spot on the TLC plate after elution in an organic solvent.

Of the three hosts investigated herein, **3** is most efficient, both in altering the aggregation properties (**6** and **10**), and in inhibiting the hydrolytic decay (**10** and **11**) of the squaraines.

Preliminary efforts towards developing a colorimetric sensing system employing the squaraine-dimer complexes resulted in the discovery of a unique visual response for benzo[a]pyrene via the combination of squaraine **10** and dimer **2**. While the free squaraine **10** undergoes hydrolysis in aqueous phosphate saline buffer (PBS) solution, a mixture of squaraine **10** + dimer **2** (1:5 molar ratio) results in a stable solution with an intense purple coloration (Figure 14). Addition of benzo[a]pyrene results in the dissipation of the intense purple hue of the solution, which exhibits a bluish coloration. This could likely be due to the competitive association of the analyte to the host **2**, thereby disrupting the pre-formed **10** + **2** complex. Current work in our laboratory is focused on establishing this detection system for selective guest analytes,

as well as investigating its sensitivity for them. The results of these investigations will be reported in due course.
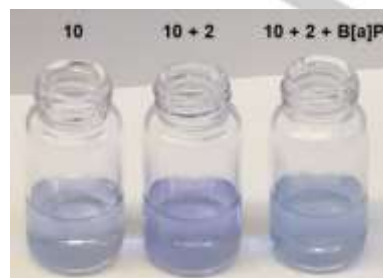

Figure 14. Visual detection of benzo[a]pyrene via squaraine **10** and dimer **2** combination (Left: aqueous PBS solution of squaraine **10** (24 μM); centre: solution of squaraine **10** (24 μM) + dimer **2** (120μM); right: squaraine **10** (24 μM) + dimer **2** (120 μM) + benzo[a]pyrene (30 μM))

Conclusions

In conclusion, we have synthesized a series of three novel β-cyclodextrin dimers. These three variable architectures have been synthesized through variation of the linker moieties tethering the two individual β-cyclodextrin units, which alters their flexibilities and associated binding properties. The incorporation of fluorescent anthracene and naphthalene units in these flexible linkers render the β-cyclodextrin dimer hosts both photophysically active and conformationally flexible. We also incorporated a rigid heteroaromatic (pyridyl group) linker to compare the host properties against the flexible dimer hosts, and observed that the structural adaptations exhibited by the flexible dimers directly enables unprecedently high association constant values for complimentary guest molecules like linear squaraine dyes. A remarkable control of photophysical properties and chemical reactivity of squaraine dyes has been shown via hydrophobic complexation with the dimer hosts in aqueous solution, which can be utilized in selective and sensitive colorimetric sensing of environmentally toxic analytes.

Experimental Section

General Information. All of the starting materials, reagents, and solvents were purchased from Sigma Aldrich, Acros Organics, TCI chemicals, Alfa Aesar, or Fisher Scientific, and were used as received. For air and moisture-free reactions, oven dried glassware, anhydrous solvent, and proper Schlenk-line techniques were employed. Reactions were monitored via analytical thin layer chromatography (TLC) using polyester-backed TLC plates. Visualization was accomplished with UV light at 254 nm. Flash column chromatography was performed with SiliaFlash F60 (230-400 mesh) or using automated flash chromatography (Yamazen Smart Flash AI-580S & AKROS). UV-VIS spectra were recorded on a Shimadzu UV-3600 Plus spectrophotometer. Fluorescence spectra were recorded on a Shimazdu RF-6000 spectrophotometer with 3.0 nm excitation slit widths and 3.0 nm emission slit widths. ^{1}H and ^{13}C NMR spectra were taken on a Bruker 400 MHz spectrometer and were recorded in D$_2$O, CDCl$_3$ or DMSO-d6 at room temperature. Chemical shifts (δ) are reported in parts per

FULL PAPER

million relative to D$_2$O at 4.79 ppm, chloroform at 7.26 ppm, dimethyl sulfoxide at 2.59 ppm, or to tetramethylsilane (TMS) at 0.00 ppm for ^{1}H NMR, and relative to CDCl$_3$ at 77.16 ppm or DMSO at 40.76 ppm for ^{13}C NMR spectra. Mass spectra for compounds **1**, **2** and **3** were recorded in a Bruker Omniflex MALDI-TOF instrument (using 2,5- dihydroxybenzoic acid as a matrix) and in a Waters Q-TOF micro-mass spectrometer at the Department of Chemistry Instrumentation Facility (DCIF) at the Massachusetts Institute of Technology (MIT), with samples run by Dr. Li Li. Mass spectra of compounds **4**, **5**, **6**, **7**, **10** and **11** were recorded on a ThermoScientific LTQ Qrbitral XL™. For further information of sample preparation, see ESI.

Spectroscopic Methods

Methods for fluorescence titration experiments. 6.25 µL of a 0.5 mg/mL (0.2 mM) aqueous solution of the host dimer (**1-3**) was added to a cuvette containing 2.5 mL of aqueous phosphate buffer solution (PBS, buffered at pH 7.4). The fluorescence spectra of this solution were measured after being titrated with solutions of the guest dyes (0.2 mg/mL solution in THF) at the following addition volumes: 0.0, 1.5, 3.0, 4.5, 6.0, 7.5, 9.0, 10.5, 12.0, 13.5, 15.0, 20.0, 30.0, 40.0 and 50.0 µL dye solutions. Each measurement was repeated for four trials. All fluorescence spectra were integrated vs. wavenumber on the X-axis using OriginPro Version 9.1. The concentration range scanned for each dye against the host concentration (approximately 0.5 µM) was further refined based on the association constant values of the host-guest combination. In particular, for association constant values greater than 10^6 M^{-1}, the guest concentration was reduced to a sub-stoichiometric (*i.e.* 0-0.5 µM) range with respect to the host. This was achieved by further diluting the stock guest solution to a final concentration of 0.04 mg/mL and adjusting the volume additions accordingly. See table S1 for final concentrations of squaraine dyes in solution

Methods for Job's plot experiments. 0.5 mg/mL of the dimer hosts in DI water and 0.04 mg/mL of the squaraine dye guests in THF were prepared separately. The fluorescence spectra of the varying concentrations of the dimer host solutions were recorded (four trials each) for the sets of mixtures (decreasing host and increasing guest) seen in Table S2. All fluorescence spectra were integrated vs. wavenumber on the X-axis using OriginPro Version 9.1. After diluting each mixture, with 2.5 mL of PBS solution in a quartz cuvette, the fluorescence spectra were recorded. Normalized fluorescence intensity (f = (F-F$_0$)/F$_0$; where F is the fluorescence intensity at a particular host concentration, and F$_0$ is the fluorescence intensity at initial concentration) was measured for each solution. Difference in f were calculated for solutions **A** (without squaraine guests) and **B** (solutions of varying concentrations of host and guest, with a fixed overall concentration of 0.5 µM). The product of Δf and mole fraction of guest (γ*Δf) is plotted against the mole fraction (γ) of guests. The mole fraction corresponding to the maxima of the plot (γ$_{max}$) was recorded.

Methods for observing hydrolysis behavior of squaraine (4-11). The absorption spectra of a mixture of 24 µM solution of host dimers (**1-3**) and 24 µM solution of guest squaraines (**4-11**) were recorded over a period of 5 hours, with spectra acquired every 30 minutes. For the 1:1 absorption spectra, 30 µL of a guest solution of squaraine (1 mg/mL in THF, 2.0 mM) and 150 µL of host solution of dimer (1 mg/mL in DI water, 0.4 mM) was added to 2.5 mL of PBS. The solution was shaken to ensure homogeneity, and the data was collected. All linear fits were done with the "Non-linear Mode Fit" command (method set to "automatic"), using the form $-\log\left[\frac{A}{A_0} - c\right] = k \cdot x$, where c, A, A$_0$, k and x refer to the integrated absorption at the aggregate concentration, concentration at time t, concentration at time zero, rate constant and the independent variable, respectively. The value of c was found from the exponential fit.

UV/vis analysis of squaraine dyes. In a quartz cuvette, the absorption spectra of a mixture of increasing concentration of squaraine guests (**4-11**), 8 µM solution of host dimers (**1-3**) added to 2.5 mL of PBS were recorded. For the absorption spectra, 50 µL of the host solution of the dimer (1 mg/mL in DI water) and increasing volumes of a 1 mg/mL solution of squaraine guests (1.5 µL; 3.0 µL; 4.5 µL; 6.0 µL; 7.5 µL; 9.0 µL; 10.5 µL; 12.0 µL; 13.5 µL; 15.0 µL) was added to 2.5 mL of PBS. The solution was shaken to ensure homogeneity and data was collected. The UV spectra were subjected to a piecewise linear background subtraction method. The selection of spectral positions to run the background were identified by a custom threshold approach. After the background spectral subtraction, the spectral signal was fitted using "Non-linear Mode Fit" command in Mathematica (method set to "automatic") with three Gaussian functions, $A \cdot Exp^{\frac{(x-\mu)^2}{2\sigma^2}}$, where A, µ, σ and x refer to the amplitude, mean, standard deviation, and wavelength, respectively.

Methods for Spectral Deconvolution and Curve Fitting

All spectral analysis was done using custom codes written in Mathematica 11.0.1.0 (Wolfram Research, Champaign, IL).

Deconvolutions. The UV spectra were subjected to a piecewise linear background subtraction method. The selection of spectral positions to run the background were identified by a custom threshold approach. After the background spectral subtraction, the spectral signal was fitted using "NonlinearModeFit" command (method set to "automatic") with three gaussian functions, $A \cdot Exp^{\frac{(x-\mu)^2}{2\sigma^2}}$, where A, µ, σ and x have their usual meanings—amplitude, mean, standard deviation, and wavelength respectively.

Linear Fits. All linear fits were done with "NonlinearModeFit" command (method set to "automatic") using the form $-\log\left[\frac{A}{A_0} - c\right] = k \cdot x$, where c, A, A$_0$, k and x refer to the integrated absorption at the aggregate concentration, concentration at time t, concentration at time zero, rate constant and the independent variable respectively. The value of c is found from the corresponding exponential fit.

Titration Curve Fits. All fluorescence titration data fits were done with Solver.xlam using "GRG-Nonlinear" method in Excel 2017 using the 1:1 and 1:2 supramolecular titration equations.

Synthetic Methods

Synthesis of all cyclodextrin hosts and squaraine guests: The conversion of β-cyclodextrin to 6-amino-6-monodeoxy-β-cyclodextrin was carried out following literature-reported procedure. [27] Naphthalene-1,4-dipropionic acid and anthracene-9,10-dipropionic acid (linkers for dimer hosts **2** and **3**) were synthesized using literature-reported procedures starting from 1,4-dimethylnaphthalene and 9,10-dimethylanthracene, respectively. [28] Bis(sucinimidyl) 2,6-pyridine carboxylate (linker for host **1**) was syntheszied using a literature-reported procedure.[29] β-cyclodextrin dimer hosts **1-3** (Figure 1) were synthesized via activated amide coupling reactions of 6-amino-6-monodeoxy-β-cyclodextrin and the bis-succinimide esters of the linkers (see ESI for more details).

1: Bis(succinimidyl) 2,6-pyridine carboxylate (50 mg, 0.14 mmol, 1.00 eq) and **S3** (350 mg, 0.31 mmol, 2.20 eq) were dissolved in 20 mL of anhydrous *N, N*-dimethylformamide under N2 and stirred at room temperature. After 24 hours, the reaction mixture was poured into approximately one liter of acetone to precipitate all cyclodextrin compounds. The precipitate was collected and washed with excess acetone and then dried under vacuum. Purification by recrystallization (acetone:water 20:80 (vol/vol)) afforded host **1** as an off-white powder (162

FULL PAPER

mg, yield = 48%). ^{1}H-NMR (400 MHz, DMSO-d_6): δ (ppm) = 3.10-3.45 (m, overlap with HDO, 29 H), 3.50-3.80 (m, 56 H), 4.23-4.62 (m, 12 H, 6-OH), 4.65-5.03 (m, 14 H, 1-H), 5.60-5.85 (m, 28 H, 2-OH & 3-OH), 8.06-8.26 (m, 3 H, ArH), 9.23–9.36 (br s, 1 H, ArNH); ^{13}C-NMR (100 MHz, DMSO-d_6) δ (ppm) = 33.44, 59.9-60.5, 71.2-73.4, 80.8-81.2, 101.6-102.0, 123.8-124.0, 125.3-125.6, 126.8-126.9, 177.7-177.8; MS (Q-TOF): m/z = 2420.72 [M + Na]$^+$ (Calculated for $C_{91}H_{143}N_3O_{70}$ + Na = 2420.76).

S11: *Bis(succinimidyl) Napthalene-1,4-dipropionic acid.* To a solution of Napthalene-1,4-dipropionic acid (100 mg, 0.37 mmol, 1.00 eq) in anhydrous *N*, *N*-dimethylformamide (2.0 mL) under nitrogen, *N*-hydroxysuccinimide (NHS, 157 mg, 1.36 mmol, 3.67 eq), *N*-(3-dimethylaminopropyl)-*N'*-ethylcarbodiimide hydrochloride (EDC, 180 mg, 0.93 mmol, 2.51 eq) and 4-(dimethylamino) pyridine (DMAP, 7.5 mg, 0.06 mmol, 0.16 eq) were added. The reaction mixture was stirred at room temperature under nitrogen overnight. After the reaction was completed (ca. 16 hours), the solvent was removed under reduced pressure. The residue was then dissolved in dichloromethane (20 mL) and this solution was washed with water (20 mL), dried with anhydrous Na_2SO_4 and evaporated to dryness under vacuum. The residue was dissolved in 1 mL of anhydrous *N*, *N*-dimethylformamide and recrystallized at 0 ºC to give **S11** as a white product (120 mg, 70% yield). ^{1}H-NMR (400 MHz, DMSO-d_6): δ (ppm) = 2.72(t, 4 H, J = 7.6 Hz, C**H**2CH2CO), 2.92 (s, 8 H, Suc-H), 3.35 (t, 4 H, J = 7.6 Hz, C**H**2CH2CO), 7.30 (s, 2 H, H- 2,3), 7.56–7.61 (m, 2 H, H-6,7), 8.07–8.11 (m, 2 H, H- 5,8), 12.29 (br s, 2 H, CO2**H**); ^{13}C-NMR (100 MHz, DMSO-d_6): δ (ppm) = 25.5, 27.4, 34.6, 124.2, 125.4, 125.8, 131.5, 135.3, 170.3, 174.5.

2: Compound **S11** (50 mg, 0.11 mmol, 1.00 eq) and 6-amino-6-monodeoxy-β-cyclodextrin (275 mg, 0.24 mmol, 2.20 eq) were dissolved in 20 mL of anhydrous *N*, *N*-dimethylformamide under N_2 and stirred at room temperature. After 24 hrs, the reaction mixture was poured into acetone (1 L) to precipitate the cyclodextrin compounds. The precipitate was collected and washed with excess acetone and then dried under vacuum. Purification by recrystallization (acetone/water 20:80) afforded dimer **2** as an off-white powder (110 mg, 40% yield). ^{1}H-NMR (400 MHz, DMSO-d_6): δ (ppm) = 2.53-2.58 (s, 4 H), 3.10-3.45 (m, overlap with HDO, 34 H), 3.50-3.80 (m, 56 H), 4.35-4.58 (m, 12 H, 6-OH), 4.75-4.90 (s, 14 H, 1-H), 5.60-5.85 (m, 28 H, 2-OH & 3-OH), 7.25-7.30 (s, 1 H, ArH), 7.50–7.60 (m, 2 H, ArH), 7.69–7.77 (br s, 1 H, ArH), 8.03-8.14 (m, 2 H, ArH); ^{13}C-NMR (100 MHz, DMSO-d_6): δ (ppm) = 25.0-25.2, 30.4-30.7, 35.5-35.7, 59.5-59.9, 71.7-73.1, 80.9-81.9, 101.6-102.0, 124.6-125.5, 128.6-128.8, 162.0-162.2; MS (MALDI-TOF): m/z = 2525.95 [M + Na]$^+$ (Calculated for $C_{100}H_{154}N_2O_{70}$ + Na = 2525.85).

S17: *Bis(succinimidyl) anthracene-9,10-dipropionic acid.* To a solution of anthracene-9,10-dipropionic acid (100 mg, 0.31 mmol, 1.00 eq) in anhydrous *N*, *N*-dimethylformamide (2.0 mL) under a nitrogen atmosphere, *N*-hydroxysuccinimide (NHS, 157 mg, 1.36 mmol, 4.39 eq), *N*-(3-dimethylaminopropyl)-*N'*-ethylcarbodiimide hydrochloride (EDC, 180 mg, 0.93 mmol, 3.00 eq) and 4-(dimethylamino) pyridine (DMAP, 7.5 mg, 0.06 mmol, 0.19 eq) were added. The reaction mixture was stirred at room temperature under nitrogen overnight. After 16 hours, the solvent was removed under reduced pressure. The residue was then dissolved in dichloromethane (20 mL) and this solution was washed with water (20 mL), dried with anhydrous K_2SO_4 and evaporated to dryness under vacuum. The residue was dissolved in 1 mL of anhydrous *N*, *N*-dimethylformamide and recrystallized at 0 ºC to give compound **S17** as a dark brown colored product (105 mg, 65% yield). ^{1}H-NMR (400 MHz, DMSO-d_6): δ (ppm) = 2.82 (t, 4 H, J=8.2 Hz, CH2C**H**2CO), 2.92 (s, 8 H, Suc-H), 3.92 (t, 4 H, J = 8.2 Hz, C**H**2CH2CO), 7.59 (dd, 4 H, Ar–H, J_1 = 3.2 Hz, J_2 = 7.0 Hz), 8.36 (dd, 4 H, Ar–H, J_1 = 3.2 Hz, J_2 = 7.0 Hz); ^{13}C-NMR (100 MHz, DMSO-d_6): δ (ppm) = 25.5, 27.4, 34.6, 130.7, 129.2, 126.7, 124.7, 170.3, 174.5.

3: Compound **S17** (50 mg, 0.10 mmol, 1.00 eq) and 6-amino-6-monodeoxy-β-cyclodextrin (250 mg, 0.22 mmol, 2.20 eq) were dissolved in 20 mL of anhydrous *N*, *N*-dimethylformamide under N2 and stirred at room temperature. After 24 hrs., the reaction mixture was poured into acetone (1 L) to precipitate the cyclodextrin compounds. The precipitate was collected and washed with excess acetone and then dried under vacuum. Purification by recrystallization (acetone/water 20:80) afforded host **3** as an off-white powder (84 mg, 33% yield). ^{1}H-NMR (400 MHz, DMSO-d_6) δ (ppm) = 2.53-2.58 (s, 4 H), 3.10-3.45 (m, overlap with HDO, 32 H), 3.50-3.80 (m, 56 H), 4.35-4.58 (m, 12 H, 6-OH), 4.75-4.90 (s, 14 H, 1-H), 5.60-5.85 (m, 28 H, 2-OH & 3-OH), 7.25-7.65 (m, 4 H, ArH), 7.65–8.40 (m, 4 H, ArH); ^{13}C-NMR (100 MHz, DMSO-d_6): δ (ppm) = 25.0-25.2, 30.4-30.7, 35.5-35.7, 59.5-59.9, 71.7-72.6, 72.6-73.1, 80.9-81.9, 101.6-102.0, 124.6-125.5, 128.6-128.8, 162.0-162.2; MS (Q-TOF): m/z = 2575.78 [M + Na]$^+$ (Calculated for $C_{104}H_{156}N_2O_{70}$ + Na = 2575.86).

Synthesis of squaraine dyes (compounds 4-11, Figure 3). A mixture of aniline (10-20 mmol, 1.00 eq), 3,4-dihydroxycyclobut-3-ene-1,2-dione (i.e. squaric acid; 0.50 eq) in 10-20 mL *n*-butanol/toluene (2:1 vol/vol mixture) was stirred at refluxing temperature for 1-2h in Dean-Stark apparatus. The reaction was allowed to cool to room temperature, after which the majority of the solvent was removed under reduced pressure. The remaining crude mixture was recrystallized using isopropanol to yield blue, green, purple, or gold crystalline dyes.

4: *2,4-Bis[4-(N-butyl, N-methylamino)phenyl]squaraine.* Yield: 60 %. ^{1}H NMR (400 MHz, chloroform-d) δ 8.38 (d, J = 9.2 Hz, 4H), 6.75 (d, J = 9.2 Hz, 4H), 3.48 (t, J = 7.6 Hz, 4H), 3.15 (s, 6H), 1.77 – 1.58 (m, 4H), 1.39 (h, J = 7.3 Hz, 4H), 0.98 (t, J = 7.3 Hz, 6H). ^{13}C NMR (101 MHz, chloroform-d) δ 188.24, 183.46, 154.22, 133.25, 119.74, 112.25, 52.60, 38.91, 29.39, 20.21, 13.88. HRMS (ESI+) Calcd. For C26H32N2O2 [M]+: 405.2537; Found: 405.2516.

5: *2,4-Bis[4-(N-pentyl, N-methylamino)phenyl]squaraine.* Yield: 51 %. ^{1}H NMR (400 MHz, chloroform-d) δ 8.38 (d, J = 9.2 Hz, 4H), 6.75 (d, J = 9.3 Hz, 4H), 3.48 (t, J = 7.6 Hz, 4H), 3.15 (s, 6H), 1.71-1.63 (m, 4H), 1.40-1.33 (m, 8H), 0.93 (t, J = 7.0 Hz, 6H). ^{13}C NMR (101 MHz, chloroform-d) δ 188.20, 183.47, 154.21, 133.25, 119.74, 112.25, 52.85, 38.90, 29.10, 26.98, 22.49, 14.00. HRMS (ESI+) Calcd. For C28H37N2O2 [M]+: 433.2850; Found: 433.2827.

6: *2,4-Bis[4-(N-hexyl, N-methylamino)phenyl]squaraine.* Yield: 52 %. ^{1}H NMR (400 MHz, chloroform-d) δ 8.38 (d, J = 9.2 Hz, 4H), 6.75 (d, J = 9.2 Hz, 4H), 3.48 (t, J = 7.6 Hz, 4H), 3.15 (s, 6H), 1.65 (q, J = 7.3 Hz, 4H), 1.40 – 1.27 (m, 12H), 0.90 (d, J = 6.7 Hz, 6H). ^{13}C NMR (101 MHz, chloroform-d) δ 188.27, 183.46, 154.20, 133.25, 119.75, 112.25, 52.87, 38.90, 31.56, 27.23, 26.63, 22.58, 14.00. HRMS (ESI+) Calcd. For C30H40N2O2 [M]+: 461.3163; Found: 461.3155.

7: *2,4-Bis[4-(N-heptyl, N-methylamino)phenyl]squaraine.* Yield: 42 %. ^{1}H NMR (400 MHz, chloroform-d) δ 8.38 (d, J = 9.2 Hz, 4H), 6.75 (d, J = 9.3 Hz, 4H), 3.46 (t, J = 7.7 Hz, 4H), 3.15 (s, 6H), 1.65 (q, J = 7.2 Hz, 4H), 1.38 – 1.25 (m, 16H), 0.89 (t, J = 7.0 Hz, 6H). ^{13}C NMR (101 MHz, chloroform-d) δ 188.17, 183.48, 154.21, 133.25, 119.74, 112.25, 52.88, 38.90, 31.75, 29.07, 27.29, 26.94, 22.58, 14.06. HRMS (ESI+) Calcd. For C32H45N2O2 [M]+: 489.3476; Found: 489.3452.

8: *2,4-Bis[4-(N-octyl, N-methylamino)phenyl]squaraine.* Yield: 45 %. ^{1}H NMR (400 MHz, chloroform-d) δ 8.38 (d, J = 9.2 Hz, 4H), 6.75 (d, J = 9.3 Hz, 4H), 3.48 (t, J = 7.6 Hz, 4H), 3.15 (s, 6H), 1.72 – 1.61 (m, 4H), 1.43 – 1.21 (m, 20H), 0.89 (t, J = 7.3 Hz, 6H). ^{13}C NMR (101 MHz, chloroform-d) δ 188.26, 183.47, 154.20, 133.25, 119.75, 112.25, 52.88, 38.90, 31.77, 29.37, 29.22, 27.28, 26.98, 22.63, 14.09.

FULL PAPER

9: *2,4-Bis[4-(N-nonyl, N-methylamino)phenyl]squaraine*. Yield: 50 %. ^{1}H NMR (400 MHz, chloroform-d) δ 8.38 (d, J = 9.2 Hz, 4H), 6.75 (d, J = 9.3 Hz, 4H), 3.48 (t, J = 7.3 Hz, 4H), 3.15 (s, 6H), 1.71 – 1.61 (m, 6H), 1.42 – 1.20 (m, 24H), 0.88 (t, J = 7.0 Hz, 6H). ^{13}C NMR (101 MHz, chloroform-d) δ 188.23, 183.47, 154.20, 133.25, 119.75, 112.25, 52.88, 38.90, 31.83, 29.51, 29.41, 29.23, 27.28, 26.98, 22.66, 14.10.

10: *2,4-Bis[4-(N-cyclohexylmethyl, N-methylamino)phenyl]squaraine*. Yield: 44 %. ^{1}H NMR (400 MHz, chloroform-d) δ 8.38 (d, J = 9.2 Hz, 4H), 6.75 (d, J = 9.3 Hz, 4H), 3.33 (d, J = 7.1 Hz, 4H), 3.17 (s, 6H), 1.78 – 1.66 (m, 12H), 1.31 – 1.11 (m, 6H), 1.06 – 0.93 (m, 4H). ^{13}C NMR (101 MHz, chloroform-d) δ 183.48, 154.51, 133.15, 112.41, 59.44, 40.32, 37.13, 31.08, 26.27, 25.83. HRMS (ESI+) Calcd. For C32H40N2O2 [M]+: 485.3163; Found: 485.3138.

11: *2,4-Bis[4-N-(tert-butylphenyl), N-methylamino)phenyl]squaraine*. Yield: 53 %. ^{1}H NMR (400 MHz, chloroform-d) δ 8.39 (d, J = 9.2 Hz, 4H), 7.37 (d, J = 8.4 Hz, 4H), 7.10 (d, J = 8.4 Hz, 4H), 6.84 (d, J = 9.3 Hz, 4H), 4.71 (s, 4H), 3.23 (s, 6H), 1.31 (s, 18H). ^{13}C NMR (101 MHz, chloroform-d) δ 189.43, 150.79, 133.41, 133.05, 126.18, 125.92, 120.29, 112.66, 55.75, 39.05, 34.55, 31.32. HRMS (ESI+) Calcd. For C40H45N2O2 [M]+: 585.3476 Found: 585.3453.

Computational Modelling

All computational modelling was done using commercially available Spartan software, version 16. To obtain the molecular models, the structures were first energy-minimized using multiple runs of molecular dynamics simulations. Next, these structures were submitted to MMF94 molecular mechanics methods, and the minimized structure from this was further optimized and minimized using a PM3-level semi-empirical force field in a gaseous medium. The energy obtained from these calculations were used to calculate the stabilization energy of the complex using the equation below[1]:

$$\Delta E_{complex} = E_{Complex} - E_{Host} - E_{Guest}$$

where $\Delta E_{complex}$ is the stabilization energy of the host-guest complex, $E_{complex}$ is the energy of formation of the host-guest complex, E_{Host} is the energy of formation of the β-cyclodextrin dimer hosts, and E_{Guest} is the energy of formation of the squaraine guest.

Acknowledgements

[1] a) B. V. K. J. Schmidt, C. Barner-Kowollik, *Angew. Chem. Int. Ed.* **2017**, *56*, 8350-8369; b) L. Szente, J. Szeman, *Anal. Chem.* **2013**, *85*, 8024-8030.

[2] a) R. Breslow, S. Halfon, *Proc. Natl. Acad. Sci. U.S.A.* **1992**, *89*, 6916-6918; b) D. C. Rideout, R. Breslow, *J. Am. Chem. Soc.* **1980**, *102*, 7816-7817; c) H.-J. Schneider, *Acc. Chem. Res.* **2015**, *48*, 1815-1822.

[3] a) L. Isaacs, *Acc. Chem. Res.* **2014**, *47*, 2052-2062; b) L. Isaacs, *Chem. Commun.* **2009**, 619-621.

[4] a) W. M. Nau, M. Florea, K. I. Assaf, *Israel J. Chem.* **2011**, *51*, 559-577.

[5] a) I.-S. Tamgho, S. Chaudhuri, M. Verderame, D. J. DiScenza, M. Levine, *RSC Adv.* **2017**, *7*, 28489-28493; b) B. Radaram, M. Levine, *Eur. J. Org. Chem.* **2015**, *2015*, 6194-6204; c) B. Radaram, J. Potvin, M. Levine, *Chem. Commun.* **2013**, *49*, 8259-8261.

[6] a) D. Ajami, J. Rebek, *Topics Curr. Chem.* **2012**, *319*, 57-78; b) D. Ajami, J. Rebek, *Acc. Chem. Res.* **2013**, *46*, 990-999; c) J. Murray, K. Kim, T. Ogoshi, W. Yao, B. C. Gibb, *Chem. Soc. Rev.* **2017**, *46*, 2479-2496; d) S. Liu, B. C. Gibb, *Chem. Commun.* **2008**, 3709-3716.

[7] T. Mako, P. Marks, N. Cook, M. Levine, *Supramol. Chem.* **2012**, *24*, 743-747.

[8] N. Serio, K. Miller, M. Levine, *Chem. Commun.* **2013**, *49*, 4821-4823.

[9] N. Serio, J. Roque, A. Badwal, M. Levine, *Analyst* **2015**, *140*, 7503-7507.

[10] D. J. DiScenza, M. Levine, *Supramol. Chem.* **2016**, *28*, 881-891.

[11] N. Serio, C. Chanthalyma, L. Prignano, M. Levine, *ACS Appl. Mater. Interfaces* **2013**, *5*, 11951-11957.

[12] a) N. Serio, D. F. Moyano, V. M. Rotello, M. Levine, *Chem. Commun.* **2015**, *51*, 11615-11618; b) N. Serio, C. Chanthalyma, L. Prignano, M. Levine, *Supramol. Chem.* **2014**, *26*, 714-721.

[13] a) D. J. DiScenza, M. Verderame, M. Levine, *Clean: Soil, Air, Water* **2016**, *44*, 1621-1627; b) D. J. DiScenza, M. Levine, *New J. Chem.* **2016**, *40*, 789-793.

[14] a) K. Iijima, D. Aoki, H. Sogawa, S. Asai, T. Takata, *Polym. Chem.* **2016**, *7*, 3492-3495; b) D.-T. Pham, H.-T. Nguyen, S. F. Lincoln, J. Wang, X. Guo, C. J. Easton, R. K. Prud'homme, *J. Polym. Sci. A Polym. Chem.* **2015**, *53*, 1278-1286; c) S. Aime, E. Gianolio, F. Arena, A. Barge, K. Martina, G. Heropoulos, G. Cravotto, *Org. Biomolecular Chem.* **2009**, *7*, 370-379.

[15] a) U. Kauscher, B. J. Ravoo, *Beilstein J. Org. Chem.* **2016**, *12*, 2535-2542.

[16] a) L. Beverina, M. Sassi, *Synlett* **2014**, *25*, 477-490; b) L. Beverina, P. Salice, *Eur. J. Org. Chem.* **2010**, 1207-1225; c) S. Sreejith, P. Carol, P. Chithra, A. Ajayaghosh, *J. Mater. Chem.* **2008**, *18*, 264-274.

[17] a) A. R. Ballestas-Barrientos, A. W. Woodward, W. V. Moreshead, M. V. Bondar, K. D. Belfield, *J. Phys. Chem. C* **2016**, *120*, 7829-7838.

[18] I.-C. Wu, J. Yu, F. Ye, Y. Rong, M. E. Gallina, B. S. Fujimoto, Y. Zhang, Y.-H. Chan, W. Sun, X.-H. Zhou, C. Wu, D. T. Chiu, *J. Am. Chem. Soc.* **2015**, *137*, 173-178.

[19] E. Hemmer, P. Acosta-Mora, J. Mendez-Ramos, S. Fischer, *J. Mater. Chem. B* **2017**, *5*, 4365-4392.

[20] a) K. T. Arun, D. T. Jayaram, R. R. Avirah, D. Ramaiah, *J. Phys. Chem. B* **2011**, *115*, 7122-7128; b) S. Das, K. G. Thomas, M. V. George, P. V. Kamat, *J. Chem. Soc. Faraday Trans.* **1992**, *88*, 3419-3422.

[21] a) Liu, T.; Liu, X.; Valencia, M. A.; Sui, B.; Zhang, Y.; Belfield, K. D. *Eur. J. Org. Chem.* **2017**, 3957-3964. b) Law, K.-Y.; Bailey, C. F. *Can. J. Chem.* **1986**, *64*, 2267-2273.

[22] a) A. J. McKerrow, E. Buncel, P. M. Kazmair, *Can. J. Chem.* **1995**, *73*, 1605-1615; b) G. Chen, H. Sasabe, W. Lu, X. Wang, J. Kido, Z. Hong, Y. Yang, *J. Mater. Chem. C.* **2013**, *1*, 6547-6552.

[23] H. Chen, W. G. Herkstroeter, J. Perlstein, K. Y. Law, D. G. Whitten, *J. Phys. Chem.* **1994**, *98*, 5138-5146.

[24] M. Narita, J. Itoh, T. Kikuchi, F. Hamada, *J. Inclusion Phenom. Macrocyclic Chem.* **2002**, *42*, 107-114.

[25] R. Breslow, S. Halfon, B. Zhang, *Tetrahedron* **1995**, *51*, 377-388.

[26] a) J. J. Gassensmith, E. Arunkumar, L. Barr, J. M. Baumes, K. M. DiVittorio, J. R. Johnson, B. C. Noll, B. D. Smith, *J. Am. Chem. Soc.* **2007**, *129*, 15054-15059; b) C. Ke, H. Destecroix, M. P. Crump, A. P. Davis, *Nat. Chem.* **2012**, *4*, 718-723; c) T. S. Jarvis, C. G. Collins, J. M. Dempsey, A. G. Oliver, B. D. Smith, *J. Org. Chem.* **2017**, *82*, 5819-5825; d) W. Liu, E. M. Peck, K. D. Hendzel, B. D. Smith, *Org. Lett.* **2015**, *17*, 5268-5271; e) E. M. Peck, W. Liu, G. T. Spence, S. K. Shaw, A. P. Davis, H. Destecroix, B. D. Smith, *J. Am. Chem. Soc.* **2015**, *137*, 8668-8671.

[27] a) M. Lovrinovic, C. M. Niemeyer, *ChemBioChem* **2007**, *8*, 61-67; b) W. Tang, S. Ng, *Nature Protocols* **2008**, *3*, 691-697.

[28] a) V. M. Cangelosi, A. C. Sather, L. N. Zakharov, O. B. Berryman, D. W. Johnson, *Inorganic Chem.* **2007**, *46*, 9278-9284; b) D. Costa, E. Fernandes, J. L. M. Santos, D. C. G. A. Pinto, A. M. S. Silva, J. L. F. C. Lima, *Anal. Bioanal. Chem.* **2007**, *387*, 2071-2081; c) D. Ryu, E. Park, D.-S. Kim, S. Yan, J. Y. Lee, B.-Y. Chang, K. H. Ahn, *J. Am. Chem. Soc.* **2008**, *130*, 2394-2395; d) Z.-Y. Zeng, Y.-B. He, J.-L. Wu, L.-H. Wei, X. Liu, L. Z. Meng, X. Yang, *Eur. J. Org. Chem.* **2004**, 2888-2893; e) Y. Fu, H. Li, W. Hu, D. Zhu, *Chem. Commun.* **2005**, 3189-3191; f) S. Icli, S. Demic, B. Dindar, A. O. Doroshenko, C. Timur, *J. Photochem. Photobiol. A Chem.* **2000**, *136*, 15-24.

[29] T. M. Postma, W. R. J. D. Galloway, G. D. Pantoú, J. E. Stokes, D. R. Spring, *Synlett* **2013**, *24*, 765-769.

FULL PAPER

Entry for the Table of Contents

FULL PAPER

Three newly synthesized β-cyclodextrin dimers have been found to complex a variety of squaraine dyes with high association constants and interesting geometries. Displacement of the squaraine dye from the cavity by an analyte provides a promising sensing platform.
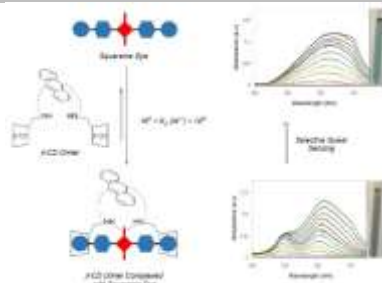
S. Chaudhuri, M. Verderame, Y. M. N. D. Y. Bandara, A. I. Fernando, T. L. Mako and M. Levine*

Page No. – Page No.

Synthetic β-cyclodextrin dimers for squaraine binding: Effect of host architecture on photophysical properties, aggregate formation and chemical reactivity